

Laser-induced fluorescence line narrowing in Eu glass: A spectroscopic analysis of coordination structure*

C. Brecher and L. A. Riseberg

GTE Laboratories, Inc., Waltham, Massachusetts 02154

(Received 21 July 1975)

By means of the techniques of laser-induced fluorescence line narrowing, the emission spectrum of Eu^{3+} in a sodium-barium-zinc silicate glass, and the temporal dependence of the emission, were measured as functions of excitation wavelength. Large variations were observed in the intensities and wavelengths of the various components of the emission. The observed transitions were assigned in terms of a C_2 site symmetry, which was found to give an adequate approximation to the symmetry of the local environment of the ion. Crystal-field calculations were performed and gave a respectable fit to the observed splitting across the entire range of pump wavelengths. A simple structural model is proposed for the behavior of the first coordination shell of the Eu^{3+} ion in the glassy matrix. The model involves the progressive approach of a ninth ligand into an originally octacoordinate site, and is consistent with the signs and relative magnitudes of the experimentally derived crystal-field parameters.

I. INTRODUCTION

A detailed understanding of the optical properties of paramagnetic ions in glasses represents one of the major gaps remaining in solid-state spectroscopy. Because an amorphous solid does not have the ordered structure normally found in crystals, the environment of a fluorescent ion is not sufficiently well defined to enable a simple characterization of its optical properties.¹ In glassy host media, the emission observed from rare-earth ions consists of a superposition of contributions from individual ions distributed among the entire ensemble of local environments. The resulting statistical distribution of Stark components brings about a significant degree of inhomogeneous broadening of the absorption and emission lines and has severely limited the numerous attempts at structural interpretation.²⁻⁶ Similar difficulties have limited the understanding of the excited-state kinetics in glassy media.⁷⁻¹⁰

The technique of laser-induced fluorescence line narrowing provides a new and powerful tool for probing the emission properties of ions in disordered systems. This technique, first demonstrated by Szabo¹¹ and later extended by Riseberg to the case of rare-earth ions in glass,¹² involves the selective excitation, within an inhomogeneously broadened absorption line, of a subgroup of ion sites narrowly defined in energy. If the emission can be measured in a time short compared with that necessary for diffusion of energy from the excited ion, the fluorescence observed is specific to that energetically defined subset and is narrowed relative to the inhomogeneous width that is normally observed.

Utilization of time-resolved techniques permits the elucidation of energy-transfer processes lead-

ing to the redistribution of the excitation throughout the entire population, and a number of such investigations have already been performed.¹³⁻¹⁸ In addition, however, observation of the line-narrowed spectra permits determination of the energy levels and hence of the crystal field influencing the selected subset. Furthermore, by excitation at various points across the inhomogeneously broadened absorption it becomes possible to map the systematic variations of the crystal field over the entire ensemble of microscopic environments in the glass and to extract information on their structural properties.

In this regard, the unique spectroscopic characteristics of the Eu^{3+} ion make it particularly appropriate for this type of experimental study. The ion has a simple energy-level structure and generally well-resolved Stark components, thus minimizing interpretational ambiguities. The emitting state cannot be split by *any* crystal field, enhancing the precision of site selectivity. Finally, the corresponding inhomogeneously broadened absorption lies at a wavelength ideal for the most powerful dye laser, rhodamine 6G. In this paper we present the results of such a study.

II. EXPERIMENTAL

The material chosen for this investigation was a sodium-barium-zinc silicate glass, a typical composition for high-power Nd^{3+} glass lasers. Two Eu^{3+} -doped samples, denoted *A* and *B*, were prepared by the National Bureau of Standards and were provided to us by Weber of the Lawrence Livermore Laboratory as part of a larger study on fluorescent properties of ions in glasses. The respective percentage compositions are as follows:

sample *A* (0.09-mol% Eu^{3+}): SiO_2 , 74.75; Na_2O , 15.0; BaO , 5.0; ZnO , 5.0; Eu_2O_3 , 0.25; and sample *B* (1.10-mol% Eu^{3+}): SiO_2 , 72.0; Na_2O , 15.0; BaO , 5.0; ZnO , 5.0; Eu_2O_3 , 3.0. Since the only major difference was in Eu^{3+} ion concentration, most of the measurements were performed on the more intensely emitting higher concentration sample *B*, with just enough attention to the other to ascertain its similarity in behavior. Unless otherwise specified, the subsequent discussion refers only to the higher concentration specimen.

The bulk of the experimental measurements were performed using the techniques of laser-induced line-narrowing spectroscopy. The basic setup is shown in Fig. 1. Excitation was accomplished with a rhodamine 6G dye laser ($1 \times 10^{-3}\text{M}$ in ethanol), which in turn was pumped by an Avco Model C 950 pulsed nitrogen laser. The dye cell is wedged to minimize the residual feedback from the cell windows. Tuning was accomplished using a Tropel collimator with antireflective optics and a PTR Optics echelle grating. The output could be tuned from 5700 to 6200 Å, and has a typical linewidth of 2 cm^{-1} . The output pulse had a peak power of approximately 10 kW, a duration of 15 nsec, and a repetition rate of 10–20 Hz. The dye laser could also be operated with broadband output extending over the entire inhomogeneously broadened absorption line (Fig. 2) by replacing the grating with a mirror.

The excitation was focused on specimens mounted in a Janis Vari-Temp Cryostat, and measurements were made at about 300, 80, and 20 K. The emission was measured with a Jarrell-Ash 1-m Czerny-Turner monochromator and detected with an RCA C31034A photomultiplier having an extended S-20 response. A PAR Model 160 Boxcar Aver-

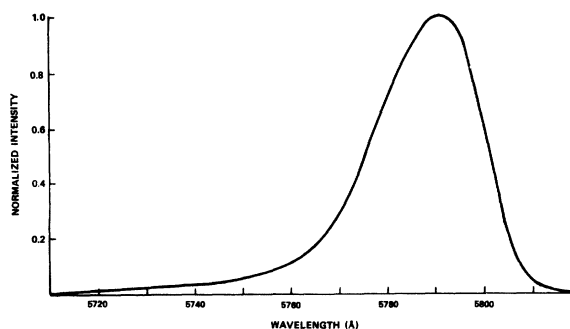


FIG. 2. Intensity profile of the inhomogeneously broadened 5D_0 - 7F_0 resonance transition of Eu^{3+} in NaBaZn silicate glass (at 80 K) used for excitation.

ager, triggered by the laser, provided electronically gated signal processing, allowing either fixed or scanned delays. Steady-state fluorescence and absorption measurements were also made using routine techniques. Spectra were measured with the laser tuned at 10 Å intervals between 5730 and 5810 Å; these are shown in Fig. 3, and the pertinent wavelengths are listed in Table I. The line-narrowing effect is immediately evident, the most striking feature being the strong shift in the lowest component of the 5D_0 - 7F_1 emission, especially when compared with the emission under broad band laser or steady-state lamp excitation (Fig. 4). This component is much sharper than the others, but some sharpening and shifts are measured in all. Similar shifts are observed in the 5D_0 - 7F_2 emission region, which shows dramatic changes in overall shape. The 5D_0 - 7F_3 and 5D_0 - 7F_4 regions have been sampled, but because of incomplete resolution are not useful in the subsequent interpretation.

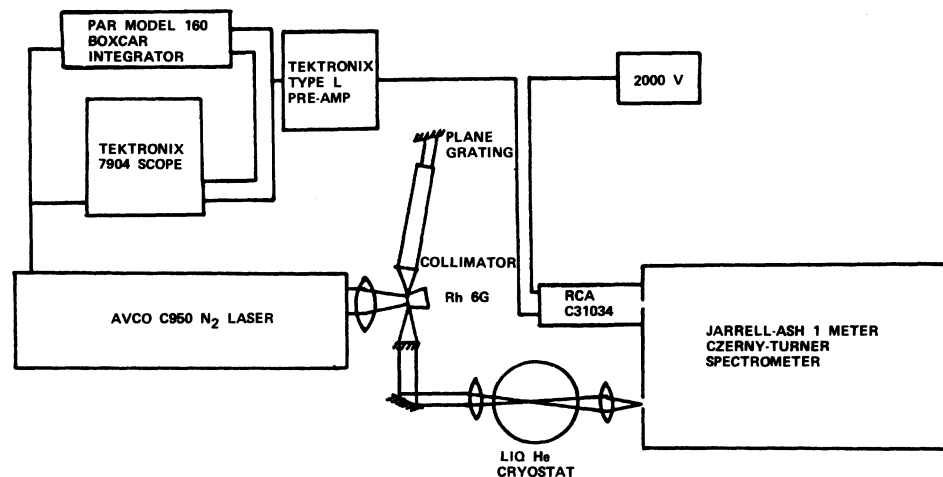


FIG. 1. Experimental apparatus for laser induced fluorescence line-narrowing measurements.

III. DISCUSSION

A. Site selectivity and energy migration

Although the line-narrowing effect is readily observable in the measured spectra, the validity of the interpretation depends rather significantly on

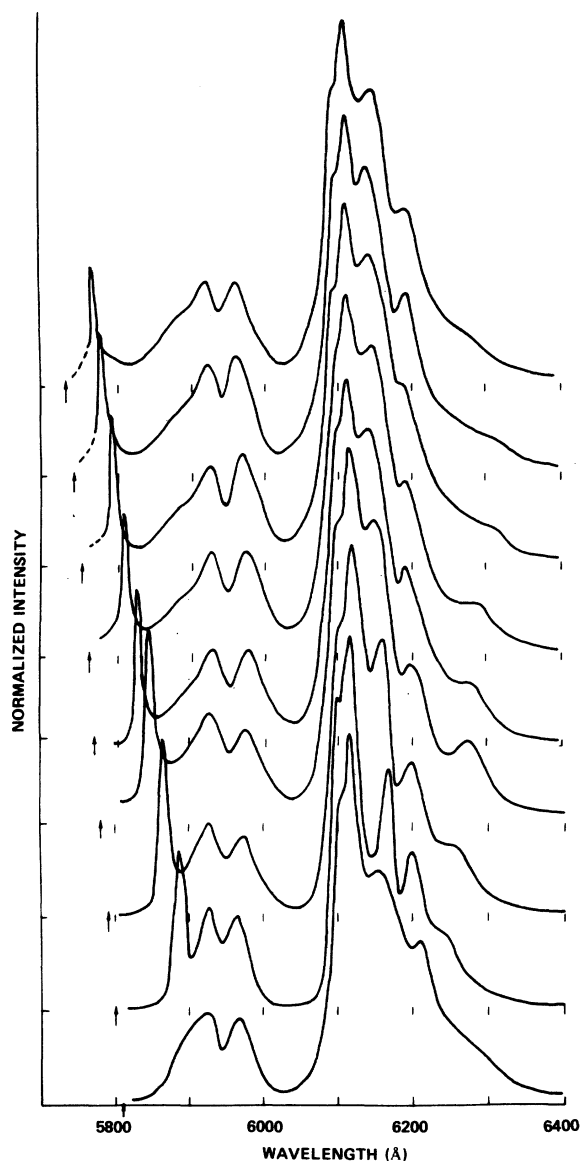


FIG. 3. Emission spectra of Eu^{3+} in NaBaZn silicate glass (at 20 K) as a function of excitation wavelength. Arrows indicate excitation, at 10 Å intervals between 5730 and 5810 Å. Delay time after excitation pulse, 100 μsec . Intensities normalized to 6113 Å peak at each pump wavelength; for approximate comparison of intensities at different pump wavelengths, multiply by the respective intensities of the pump transition, Fig. 2.

the degree of site selectivity that this in fact represents. This site selectivity can be degraded in a number of ways. Simplest among these is non-monochromaticity of the exciting radiation. The rhodamine 6G dye laser has such a high intrinsic gain that it is impossible to suppress entirely the untuned broadband emission caused by superradiance and stray nonselective feedback. The peak intensity of this emission is some three orders of magnitude below that of the tuned line of the laser; since its bandwidth is a factor of 100 greater, however, it can contribute significantly to the total exciting radiation falling on the sample. The contribution can be ascertained by blocking the feedback from the grating and measuring the residual fluorescence from the sample. The contribution is not important except at the extremes of the pump wavelength range, where it can be as much as 20% of the line-narrowed signal.

Another cause of degradation of the site selectivity is energy migration. This effect is demonstrated in Fig. 5, which shows the deterioration of the line-narrowing effect as the delay time of the measurement is increased from 50 μsec to 5 msec. Note that the respective spectra change toward that measured under broadband excitation (Fig. 4), of which the shoulder at about 5880 Å is the most readily distinguishable feature. The fact that the latter is observed only 50 μsec after excitation even at 20 K, while some line narrowing persists 5 msec later (and even at 300 K in the more dilute sample) indicates a remarkably broad range of cross-relaxation times. We do not choose to consider this question in detail; let it suffice to say that the incremental degradation of the line-narrowed signal is small, and that at times short compared to the fluorescence decay (as in most of our measurements), the line-narrowed spectrum constitutes the bulk of the contribution.

A final question concerns the remaining degree of inhomogeneity in the measured spectra. In the subsequent discussion it is assumed that the energy of that 5D_0 state pertinent to a particular spectrum is defined by the energy of the pump line, and that conversely the rest of the spectrum is characteristic of the single class of sites selected. Although it is conceivable that two or more sites differing widely in their crystal-field properties may have the same ${}^5D_0 - {}^7F_0$ energy, we observe no line-narrowed components whose interpretation requires a second site. The homogeneous widths should be large,¹⁰ however, as expected from the high density of low-energy phonons in glass; any residual inhomogeneous contribution [as reported in the $\text{Ca}(\text{PO}_3)_2$ glass system¹⁶] would be considered unimportant as long as it does not change the measured position of the component.

TABLE I. Emission wavelengths of Eu^{3+} in NaBaZn silicate glass as functions of pump wavelengths.

Pump wavelength (Å)		Emission wavelengths (Å)						
5810	5911	5925	5959	6101	6113	6169	6199	6244
5800	5888	5925	5965	6100	6113	6162	6198	6256
5790	5867	5926	5971	6099	6113	6157	6197	6266
5780	5846	5926	5975	6098	6113	6153	6197	6274
5770	5827	5925	5976	6097	6112	6151	6198	6277
5760	5810	5924	5974	6096	6112	6150	6199	6273
5750	5793	5923	5970	6095	6111	6150	6199	6267
5740	5778	5922	5966	6054	6111	6150	6199	6260
5730	5764	5920	5962	6092	6110	6149	6197	6252

B. Assignment and interpretation

The disordered nature of the glassy matrix presents a major impediment to the interpretation of the spectra. The lack of anything higher than trivial (C_1) symmetry removes all selection rules, allowing all transitions to appear in all directions; furthermore, the lack of long-range correlation between sites prevents the use of polarization behavior as a criterion for establishing the identity of a given transition. Nevertheless, certain features common to the entire set of spectra indicate that some degree of local order persists in the immediate environment of the emitting ion. We observe, for example, that although the emission from the 5D_0 level to the 7F_1 and 7F_2 states are split into the maximum number of components (three and five, respectively), these components differ markedly in their behavior. In the 7F_1 region, for example, the shortest wavelength component is considerably sharper than the other two and its location is much more sensitive to the pump wavelength. In the 7F_2 region, the lower three components are substantially more intense than the other two and shift less in energy. And finally there is a clear systematic correspondence between the respective spectral components at different excitation wavelengths.

In view of these points, we feel it appropriate to assign the spectra in terms of an average local symmetry in which the immediate environments of the ions are assumed to share a degree of short-range order common to all, and that the lowering of symmetry below this level in the bulk reflects largely the randomness of orientation from one site to the next. For this treatment the most appropriate symmetry is C_{2v} : It is the highest symmetry in which full splitting of the 7F_1 and 7F_2 levels is allowed while maintaining symmetry-based distinctions between almost all the compo-

nents. This point group allows optical activity for the three 5D_0 - 7F_1 components and for four of the five 5D_0 - 7F_2 components. It is a subgroup of almost all of the higher point symmetries in which rare-earth ions are normally found, enabling application of the standard technique of descending symmetries.¹⁷ And finally, it is the lowest symmetry for which simple crystal-field calculations can be routinely performed. The importance of

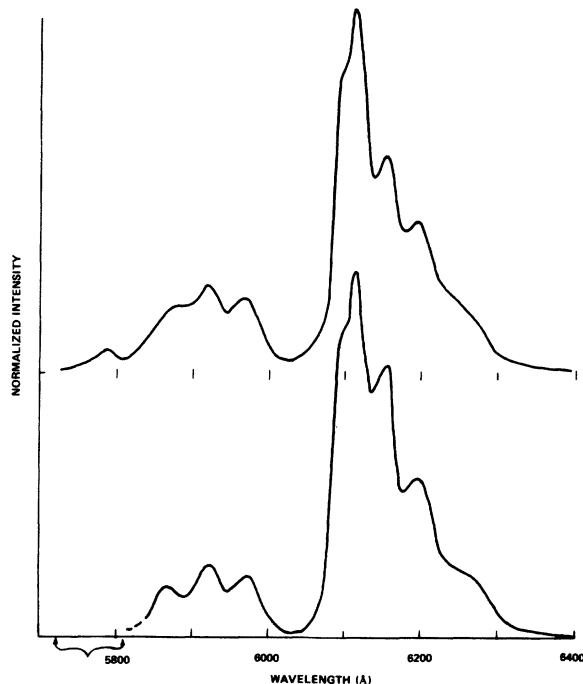


FIG. 4. Emission spectra of Eu^{3+} in NaBaZn silicate glass (at 80 K) under broadband excitation. Upper spectrum, continuous excitation in 3900 Å region; lower spectrum, pulsed excitation by free-running (untuned) dye laser emitting in broadband over full range of 5D_0 - 7F_0 absorption (indicated by arrows).

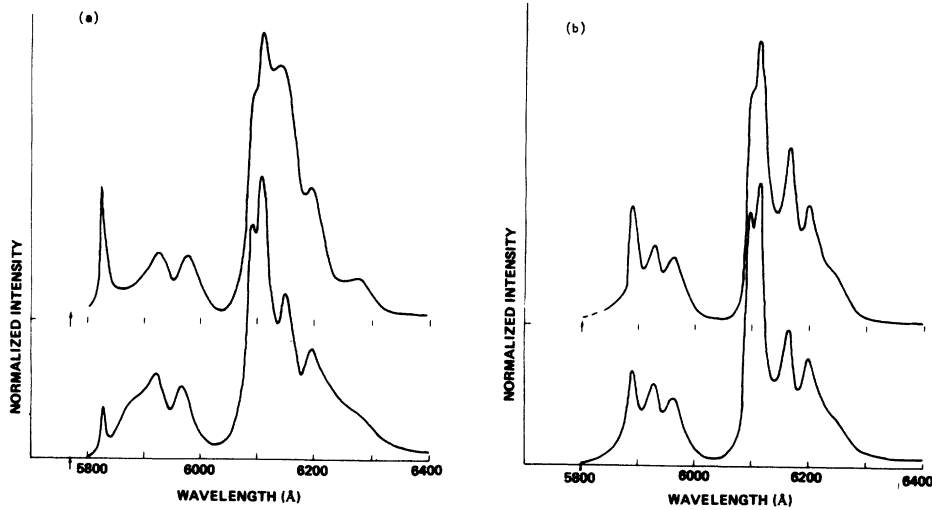


FIG. 5. Emission spectra of Eu^{3+} in NaBaZn silicate glass (at 80 K) as a function of delay time after excitation pulse. (a) Excitation at 5770 Å; (b) excitation at 5800 Å. Upper spectrum in each case measured at 50 μsec delay, lower spectrum at 5 msec delay.

TABLE II

CORRELATION MAPPINGS AND SELECTION RULES FOR THE RELEVANT SYMMETRIES

Groups:	D_{4d}	C_{4v}	C_{2v}
Irreducible representations ^a and functions belonging to them:	A_1	x^2, x^2+y^2	x^2, x^2+y^2
	A_2	R_x	R_x
	B_1	z	x^2-y^2
	B_2	(x^2-y^2)	xy
	E_1	(xy)	x
	E_2	(x)	y
	E_3	$(R_x)(x_z)$	$(R_x)(R_y)$
Transitions	Representations ^b to which transitions belong		
0-0	A_1	A_1	A_1
0-1	$A_2 + E_3$	$A_2 + E$	$A_2 + B_1 + B_2$
0-2	$A_1 + E_1 + E_3$	$A_1 + B_1 + B_2 + E$	$2A_1 + A_2 + B_1 + B_2$

^aBecause of nonstandard orientations of the coordinate axes, the representations for group D_{4d} differ from those usually found. The coordinate axes are contained in reflection planes rather than rotations, so as to facilitate correlation to C_{4v} .

^bRepresentations underlined are those for which optical activity is allowed; magnetic dipole for the 0-1 transition, electric dipole elsewhere.

this last point will become evident below.

As a starting point, the unique behavior of the shortest wavelength component of the 5D_0 - 7F_1 transition assumes considerable importance. This component, much sharper than the others and shifting more than 100 Å as a function of pump wavelength, is assigned to the transition terminating in the $M_J = 0$ level of the 7F_1 . This level is nondegenerate in all axial symmetries higher than C_1 and does not mix with any of the other levels until all axial symmetry is removed. In C_{2v} the level belongs to the A_1 representation; the other two therefore belong to the B_1 and B_2 representations, although the ordering remains ambiguous.

In the 7F_2 region we observe that the three shorter wavelength components are consistently more intense and shift less in wavelength than the other two. By the descending symmetries argument,¹⁷ we take this to be indicative of some residual higher axial symmetry. Following the point group correlations (Table II), the best set of assignments identifies the terminal level of the three shorter wavelength components as A_1 , B_1 , and B_2 , while the other two fall into A_1 and A_2 . Again the ordering is ambiguous.

In order to choose among the 24 combinations of assignments consistent with the above argument, we apply elementary crystal-field calculations. In

view of the limitations of such calculations and the approximations already made, it would be difficult to justify this approach for any single set of energies. In this case, however, we do not have merely nine unrelated spectra, but rather a basic continuity, in which the overall intensity relationships are maintained and the location and shape of individual components can be followed as continuous functions of the pump wavelength. We therefore must disregard best fits that require discontinuous changes in assignment as the pump wavelength is scanned, and instead seek a best assignment common to the entire set. We also disregard assignments for which the fit is substantially better at one end of the pump wavelength range than at the other. Applying these additional criteria we find only two sets of assignments that are at all acceptable; the better of these, with the observed and calculated energies, is listed in Table III. The pertinent crystal-field parameters are listed in Table IV.

In order to generate a geometric model for the structure of the immediate environment of the emitting ion, a number of additional assumptions are necessary. Since the number of ligands is unspecified, we assume as a starting point that, in the absence of lattice-imposed constraints to the contrary, the bulk of the Eu^{3+} ions resides in

TABLE III. Energy levels of Eu^{3+} in NaBaZn silicate glass as functions of pump wavelength assignment (in terms of C_{2v} symmetry).

Pump wavelength (Å)	7F_1			7F_2				
	A_2	B_1	B_2	A_1	A_1	A_2	B_1	B_2
5810 obs.	294	334	430	853	1196	1080	821	1002
calc.	295.3	326.0	436.1	869.2	1177.0	1083.4	802.9	1015.9
5800 obs.	258	364	477	883	1257	1107	848	1013
calc.	257.3	354.3	487.7	904.6	1230.1	1105.3	825.8	1037.3
5790 obs.	227	396	524	913	1312	1134	875	1029
calc.	224.2	388.3	535.9	934.9	1284.6	1126.4	857.5	1056.0
5780 obs.	195	426	565	942	1362	1164	902	1049
calc.	191.4	421.3	575.2	960.5	1338.9	1154.1	891.3	1072.1
5770 obs.	170	453	597	970	1400	1197	930	1074
calc.	166.9	450.6	604.0	983.0	1383.8	1188.6	924.5	1090.0
5760 obs.	149	481	622	1000	1420	1229	957	1101
calc.	147.9	480.5	624.1	1004.0	1415.0	1226.1	955.8	1105.8
5750 obs.	129	508	641	1027	1435	1260	984	1131
calc.	130.6	508.4	638.2	1021.5	1441.9	1264.3	985.0	1124.6
5740 obs.	115	535	660	1058	1447	1290	1012	1161
calc.	119.9	535.6	652.1	1041.9	1467.1	1303.4	1013.3	1143.0
5730 obs.	103	560	679	1085	1457	1315	1037	1189
calc.	111.5	560.1	666.1	1058.1	1490.6	1338.2	1037.2	1159.8

sites of eightfold coordination. With few exceptions such behavior is characteristic of Eu^{3+} in oxide-type media and is consistent with considerations of relative ionic size (0.7:1) and number of available bonding orbitals (nine). We treat the eight immediate ligands as if they were equidistant from the central ion and disregard as insignificant the contributions to the crystal field of any other neighboring ligands lying at more than twice the primary distance.¹⁸

Next we observe that the most efficient packing of eight unit spheres around a central sphere of radius roughly $\frac{2}{3}$ is the square Archimedean antiprism, symmetry D_{4d} [Fig. 6(a)]. Taking this uniaxial arrangement as the parent structure for a descending symmetries treatment, we perform a continuous and gradual distortion, systematically removing symmetry elements to reach the desired lower biaxial symmetry of C_{2v} .¹⁹

The nature and magnitude of this distortion can be extracted from the derived crystal-field parameters, each of which can be expressed as the product of two factors: the relevant tesseral harmonics (which contain the bulk of the orientational information); and a scaling factor involving charge magnitude, coordination distance, and radial expectation values for the $4f$ electrons. We choose to disregard the latter factor, and extract the pure orientational information by considering ratios of the parameters of the same order; e.g., B_{22}/B_{20} , B_{44}/B_{40} . These values can be calculated for any appropriate geometrical arrangement of eight ligands; however, when compared with the corresponding experimentally determined values, reasonable agreement can be achieved only at the long excitation wavelength limit of the set. The corresponding structure is shown in Fig. 6(b). For successively shorter excitation wavelengths the disagreement rapidly becomes intolerable; indeed, we are unable by any systematic distortion to generate a reasonably close-packed eightfold coordination structure whose calculated crystal-field parameters

behave in the appropriate manner. To resolve this inconsistency, we direct our attention to the massive changes in the mean energies of the various spin-orbit states. For example, the barycenters of the 7F_1 and 7F_2 states shift in energy by more than 25% over the range of excitation wavelengths. Such shifts, although clearly beyond the realm of elementary electrostatic crystal-field theory (which deals only with splittings from the barycenters and does not cover finer interactions, such as J -mixing), clearly imply a substantial and systematic increase in the total external field influencing the ions excited at the shorter wavelengths. This is consistent with the parallel decrease observed in the radiative lifetimes at the shorter wavelengths (see Sec. III C). Even more significant is the total breadth of the 5D_0 state, which, as seen from the absorption profile (Fig. 2) spans an energy range of some 300 cm^{-1} . In other host systems, where shifts one-tenth this amount are considered large, such shifts have always been associated with changes in the chemical nature of the environment; that is, in the number or the bonding properties of the coordinating ligands.²⁰ The disordered nature of the glassy host gives all the more reason to expect similar effects in the case at hand.

We propose, therefore, to treat the set of spectra in terms of a systematic decrease in the average distance of a ninth coordinating ligand. We consider this the most appropriate treatment for a number of reasons

(a) The relative ionic radii are appropriate ($r_{\text{Eu}^{3+}} : r_{\text{O}^{2-}} = 0.7:1$). Close-packed ninefold coordination requires only a (2–3)% increase in the mean radial distance to equivalent coordinators over that required for the corresponding close-packed eightfold coordinated structure.

(b) The medium is dilute in terms of Eu^{3+} (approximately 1 mol%) and thus oxygen rich in terms of ligands available for coordination. The Eu^{3+} ion has sufficient empty orbitals available for bonding

TABLE IV. Calculated crystal-field parameters for Eu^{3+} NaBaZn silicate glass.

Pump wavelength (\AA)	Crystal-field parameters (cm^{-1})						
	\bar{E}_1	\bar{E}_2	B_{20}	B_{22}	B_{40}	B_{42}	B_{44}
5810	352.5	989.5	-143.0	275.2	-128.2	1065.9	375.5
5800	366.4	1020.6	-272.7	333.7	-119.0	1108.1	97.6
5790	382.8	1051.9	-396.4	368.9	-105.6	1085.9	-172.7
5780	395.9	1083.4	-511.4	384.7	-94.7	1029.4	-381.7
5770	407.2	1114.0	-600.7	383.6	-86.2	968.0	-489.6
5760	417.5	1141.4	-674.0	359.1	-78.6	886.8	-523.4
5750	425.7	1167.4	-737.9	324.5	-69.6	817.8	-524.3
5740	435.9	1193.7	-789.8	291.3	-64.7	750.9	-504.4
5730	445.9	1216.8	-836.0	265.1	-60.5	701.4	-483.6

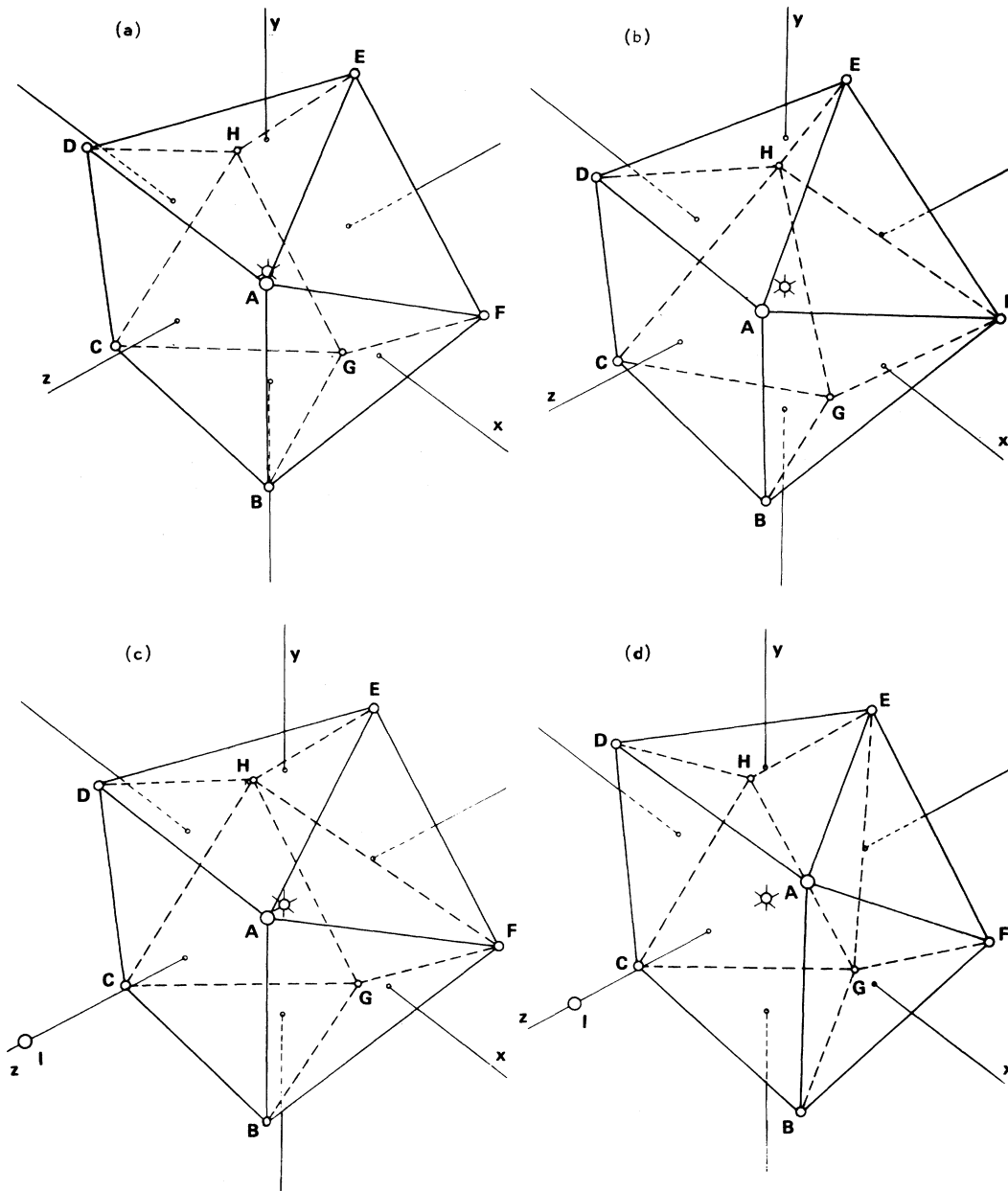


FIG. 6. Geometric models for the environment of the Eu^{3+} ion in NaBaZn silicate glass. The Eu^{3+} ion is depicted at the origin, and the eight equiradial coordinating oxygens are shown as located at the vertices of the solid geometric figure defined by connecting their centers. Structures are drawn in perspective as viewed approximately from the $[111]$ direction, with the coordinate axes shown where they emerge from the solid figure. The square Archimedean antiprism is shown in (a), with points A, B, C, D , and E, F, G, H forming two squares perpendicular to the z axis. Best-fitting pure eightfold structure is shown in (b), which is derived from (a) mostly by motion of points F and H in the $-z$ direction. The structure remains essentially unchanged by the approach of the ninth coordinator I along the z axis, until its radial distance decreases to 1.4 times that of the other eight coordinators. Closer approach requires a spatial rearrangement of the latter, which can be expressed in terms of a parameter ϵ , the fraction of the remaining decrease in distance needed to achieve equiradial ninefold coordination. Structures (c) and (d) correspond to ϵ values of 0.1 and 0.9, respectively. Note the major distortions: $ABCD$ becomes larger and rectangular ($AB=1.05 \times AD$), and points E and G move beyond points F and H in the $-z$ direction.

(sp^3d^5), and will accept the maximum coordination allowed within the constraints of the glassy network.

(c) The requisite gradual coordination change can take place within the context of an overall C_{2v} local symmetry. This gives a geometrical rationalization for the observed consistency in intensity patterns and continuity in component identification despite the rather large shifts in energy.

We therefore generate the following model for the average structure of the Eu^{3+} sites in the glassy host: Beginning with eight approximately equidistant oxygens in a geometric arrangement of a slightly elongated Archimedean antiprism we allow a ninth oxygen to approach along the twofold symmetry axis. The other eight shift their position to accommodate the intruder, until at the completion of the process all nine are approximately equidistant from the Eu^{3+} ion. The process is a continuous one, and can be described through a distortion parameter ϵ , having limiting values of zero (pure eightfold coordination) and unity (fully transformed to ninefold, equidistant coordination). Two stages are shown in Figs. 6(c) and 6(d).

Crystal-field parameters can be calculated for the various geometrical arrangements associated with the respective values of the distortion parameter ϵ . As shown in Table V and Fig. 7, the agreement with the experimentally determined values is remarkably good. All the parameters increase or decrease in the appropriate manner as a function of ϵ , and all have the appropriate signs throughout. One, the B_{42} parameter, is considerably smaller in magnitude than the measured value; this parameter, however, is the least precise of the set, entering only in the exchange terms in the calculations for the experimental fit. The B_{44} value does, in fact, change sign as predicted. The best agreement is in the major ratios (Fig. 8): As ϵ increases from 0 to 1, B_{22}/B_{20} decreases by a factor of 8 and B_{44}/B_{40} increases more than 15-fold, changing sign in the process. The values agree sufficiently well to enable a correlation between pump wavelength and distortion parameter (Fig. 9). An even better agreement could be obtained if we were to remove some of our self-imposed limitations from the model, such as equidistance for the eight primary coordinators, but such further refinement would not be useful. The agreement is most respectable as it stands, and we feel that the simple model described gives a reasonable approximation for the site variation behavior in this glassy medium.

C. Decay times

In an attempt to shed additional light on the nature of the multiple sites in the glass, measure-

ments were made of the fluorescence decay as a function of pump wavelength. If the sites selectively excited by the pump light are as distinct as indicated by the spectra, the structural differences should be reflected in characteristic differences in the fluorescence decay time. This is indeed the case, with the apparent decay times becoming increasingly shorter as the wavelength of the pump is decreased. The picture revealed by these measurements is, however, somewhat clouded; in all cases, at both liquid-nitrogen and liquid-helium temperatures, the decay curves are distinctly non-exponential. This is clearly to be expected, in view of the spectroscopic evidence (discussed earlier) that a significant degree of non-line-narrowed emission underlies all the ostensibly line-narrowed spectral components. In order to extract the information relevant to the particular site in question, further processing is required.

One approach is simply to accept the nonexponential behavior and to fit the resultant curved plot of $\ln I$ vs time by including a quadratic term:

$$\ln I = \ln I_0 - \alpha t + \beta t^2.$$

As long as the linear coefficient α remains relatively large compared with βt (short time limit), we can extract the value of the faster lifetime $\tau = 1/\alpha$ with a reasonable degree of confidence.

A better approach, in principle, would be to correct for the underlying (long-lived) background. The line-narrowed spectral components, although generally broader than would be desired, are still

TABLE V. Crystal-field ratios for various structures and pump wavelengths.

Distortion parameter (ϵ)	Pump wavelength (\AA)	B_{22}/B_{20}	B_{44}/B_{40}
0		-2.05	-0.61
	5810	-1.92	-0.93
0.1		-1.27	-0.12
	5800	-1.22	-0.82
0.3		-1.00	+0.83
	5790	-0.93	1.64
0.5		-0.91	1.63
0.7		-0.83	2.59
	5780	-0.75	4.03
0.8		-0.75	3.71
	5770	-0.64	5.68
0.9		-0.54	6.45
	5760	-0.53	6.66
	5750	-0.44	7.53
	5740	-0.37	7.80
	5730	-0.32	7.99
1.0		-0.23	9.56

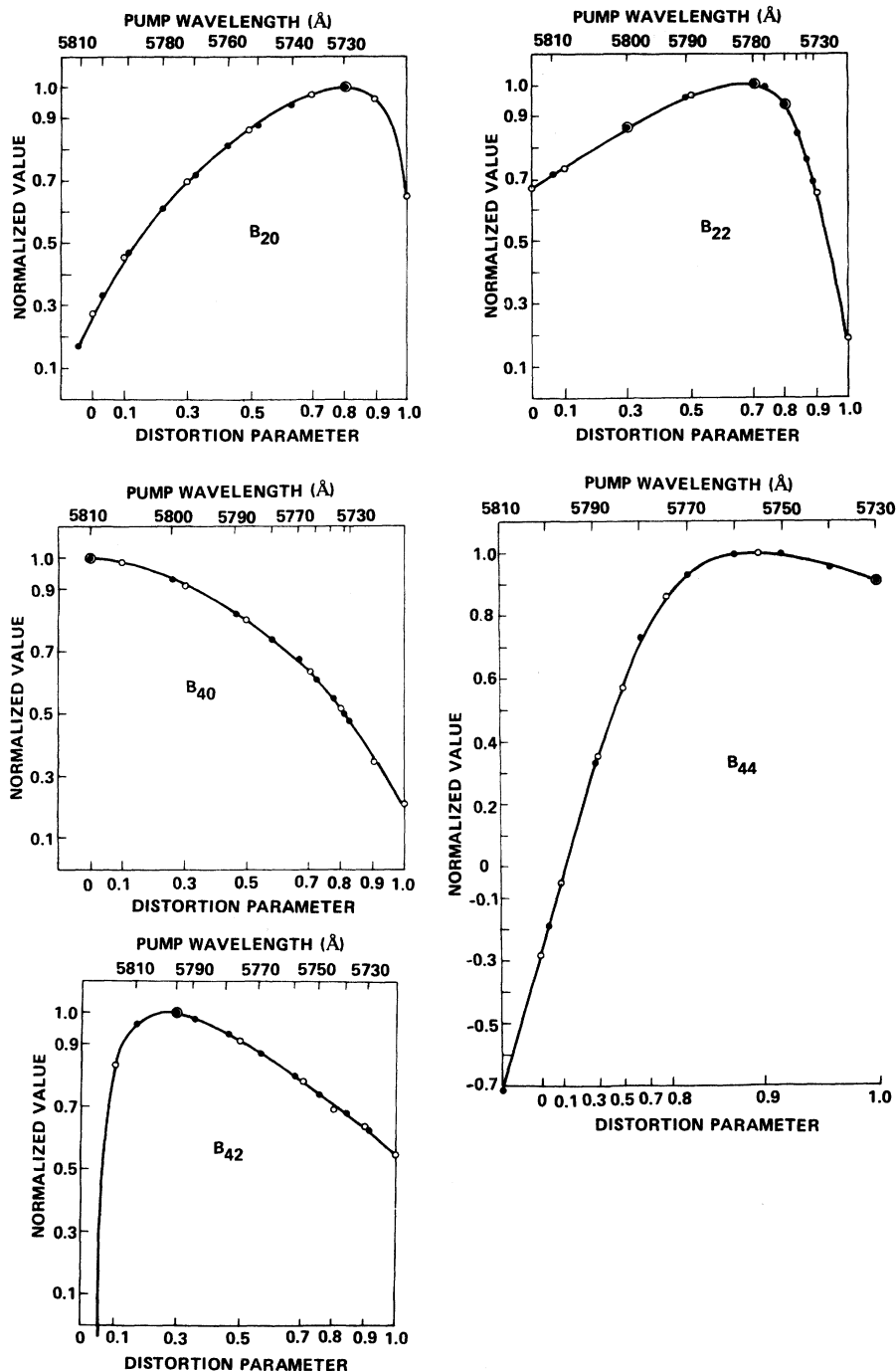


FIG. 7. Behavior of the crystal-field parameters B_{20} , B_{22} , B_{40} , B_{42} , and B_{44} as functions of pump wavelength and distortion parameter. Symbol \bullet indicates experimental measurement, \circ indicates calculation from geometric model. Values normalized with respect to maximum value in each case. Note that in all cases there is a monotonic relationship between distortion parameter and wavelength, and that both measured and calculated values span roughly the same range.

considerably sharper than those excited under non-line-narrowing conditions (broadband pulse or continuous). We therefore approximate the decay curve of the non-line-narrowed contribution underlying the component in question by the arithmetic mean of decay curves measured 20 Å on either side of the peak; this is then subtracted from the

corresponding measurements at the peak wavelength, yielding a decay curve that arises essentially from the line-narrowed component alone. Of the eight spectral components only two—the highest and lowest members of the 5D_0 - 7F_1 set—are sufficiently well resolved throughout the range of pump excitation to justify this treatment. The

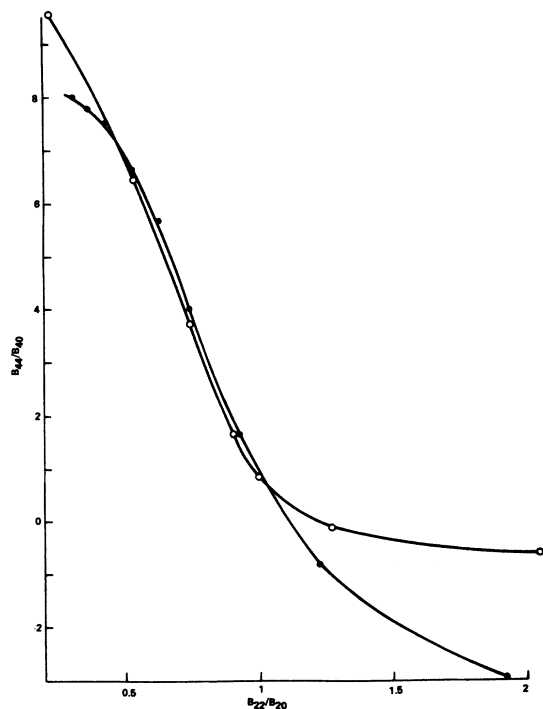


FIG. 8. Behavior of the major crystal-field ratios B_{22}/B_{20} and B_{44}/B_{40} . Symbol ● indicates experimental measurement, symbol ○ indicates calculation from geometric model. Unlike Fig. 7, these are ratios of the actual values of the respective parameters, and carry the full geometric information. Note the substantial agreement except at the most extreme cases; only the described model gives agreement over such a wide range.

decay values derived from this approach, however, agree to within 10% with those obtained from the first approach, and are not reported separately.

The decay times of the 5D_0 state were determined at all pump wavelengths of interest, and are summarized in Table VI and Fig. 10. Measurements were made at the wavelengths of the various line-narrowed components of the emission; these should, of course, be redundant, the overall lifetime of the 5D_0 state being independent of the particular transition measured. In fact, however, a systematic discrepancy is observed between the lifetime values derived from the shortest wavelength component of the line-narrowed ${}^5D_0-{}^7F_1$ transition and the values derived from the others. This component consistently exhibits a shorter lifetime, and the discrepancy increases as the pump wavelength is decreased. We attribute the discrepancy to the uniquely high spectral reso-

lution of the component, superimposing the strongest and sharpest line-narrowed contribution upon the most diffuse non-line-narrowed background. Since the long-lived background (≈ 2.2 msec) would tend to distort the line-narrowed measurements toward higher values (with greater distortion for shorter lifetime value), and the treatment depends on our ability to separate this contribution, we accept the lower values as the true measure of the decay times of the 5D_0 state.

The most significant point about the decay times is their systematic behavior as a function of pump wavelength. The decay time is a maximum at a pump wavelength of 5800 \AA , decreasing gradually and monotonically to less than $\frac{1}{3}$ of this value at the short-wavelength limit of the pump. A corresponding but precipitous drop occurs toward the long-wavelength pump limit, the decay time decreasing by at least a factor of 4 in only 10 \AA . These measured values presumably correspond to the radiative lifetimes, since the total emission intensity at any given pump wavelength is very nearly proportional to the absorbed pump energy, as determined from the absorption constant and the laser beam intensity.

To explain the behavior of the lifetimes at pump

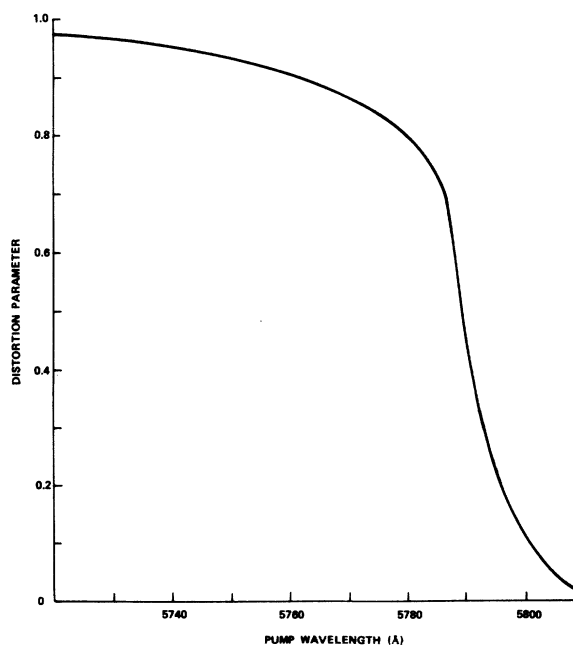


FIG. 9. Relation between pump wavelength and distortion parameter ϵ . Values extracted by interpolation along curves in Fig. 8. Note the roughly sigmoid approach to ninefold coordination.

TABLE VI. Decay times of Eu^{3+} fluorescence in NaBaZn silicate glass.

Pump wavelength (\AA)	Decay time (msec) lowest 7F_1 component	Decay time (msec) highest 7F_1 component
5810	0.64	0.59
5808	1.09	1.12
5805	1.88	1.84
5800	2.18	2.18
5790	1.95	2.12
5780	1.56	1.98
5770	1.21	1.79
5760	0.94	1.42
5750	0.77	1.15
5740	0.62	0.88
5730	0.45	0.79

wavelengths 5800 \AA and below is quite straightforward. The progressive increase in the corresponding radiative transition probabilities parallels the apparent increase in the total crystal field, particularly that of the second-order term B_{20} . In addition, it is quite consistent with the geometric model previously described, which postulates an increase in the number of ligands in the first coordination sphere. The accompanying rearrangements also increase the magnitude of the odd terms in the crystal field (particularly B_{30} , B_{32} , and B_{50} , which show increases greater than a factor of 4), implying a consequent increase in the electric dipole transition possibilities. We consider this predicted increase to be supportive of the model.

The lifetime behavior at pump wavelengths longer than 5800 \AA is more difficult to understand. Presumably the radiative lifetime should continue to increase as the magnitude of the total crystal field decreases. Note, however, that at the shorter pump wavelengths (the high-field sites) the emission corresponding to the lowest 5D_0 - 7F_1 component has shifted below the long-wavelength limit of the 5D_0 - 7F_0 pump line. Furthermore, the energy of the lowest Stark component of the 7F_1 state in the high-field sites is little more than 100 cm^{-1} above ground, so that even at liquid-nitrogen temperature that level contains some (10–15)% of the total population of those sites. Thus as the absorption owing to the direct 5D_0 - 7F_0 transition in low-field sites drops off above 5800 \AA , the absorption at the same wavelength owing to the 5D_0 - 7F_1 transition in high-field sites may become dominant. The measured lifetime should then decrease to values characteristic of the latter sites. This is supported by the observation of an anti-Stokes line-narrowed 5D_0 - 7F_0 emission at the appropriate wavelengths corresponding to the high-field sites

excited by the 5D_0 - 7F_1 absorptions. The persistence of the effect, at a diminished level, even near liquid-helium temperature indicates that some unspecified energy transfer process may also be a

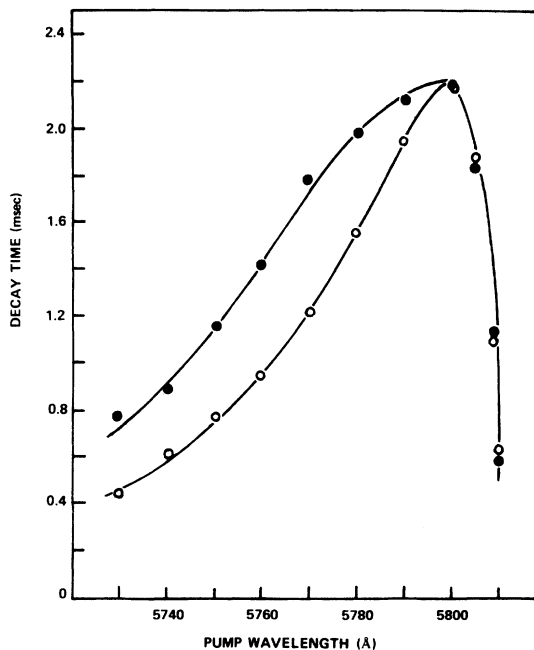


FIG. 10. Decay time of fluorescence of Eu^{3+} in NaBaZn silicate glass (at 20 K) as a function of pump wavelength. Symbol \bullet indicates measurements of longest wavelength component of 5D_0 - 7F_1 transition; symbol \circ , shortest wavelength component. While the discrepancy indicates a residue of unresolved longer-lived non-line-narrowed contribution in the former case, the parallel decrease with pump wavelength confirms that the major contribution is indeed the line-narrowed emission.

contributing factor. As indicated earlier, the question of energy migration is complex, and will be treated elsewhere^{14,15} but the lifetime behavior presents no major inconsistencies with the structural interpretation.

IV. CONCLUSION

The spectroscopy of Eu^{3+} in glass has been partially clarified by applying the techniques of laser induced line narrowing to the inhomogeneously broadened emission. The components of the emission, excited at various pump wavelengths, have been assigned and their decay times measured. From these measurements the corresponding energy levels within the 7F_1 and 7F_2 multiplets were ascertained and the functional dependence of the crystal field was calculated over the range of sites selected by the pump wavelengths.

To provide a physical rationalization for the be-

havior of the crystal-field parameters, a geometric model was generated. This model involves a gradual change from eightfold to ninefold coordination in the immediate environment of the Eu^{3+} ion, while maintaining an overall C_{2v} symmetry throughout. The model predicts crystal-field parameters whose behavior agrees well with the experimentally derived values, and we feel that it gives a reasonable approximation to the average structure of the emitting site.

ACKNOWLEDGMENTS

The authors wish to express their gratitude to M. J. Weber for many helpful discussions and his deep interest in and support of this work. We thank W. M. Yen, J. A. Paisner, and H. Samelson for their useful advice and suggestions, and B. W. Hawkins and J. Walsh for their expert technical assistance.

*Supported in part by Lawrence Livermore Laboratory.

¹J. A. Prins, in *Physics of Non-Crystalline Solids*, edited by J. A. Prins (Wiley, New York, 1965), p. 1.

²D. K. Rice and L. G. DeShazer, *Phys. Rev.* **186**, 387 (1969).

³M. M. Mann and L. G. DeShazer, *J. Appl. Phys.* **41**, 2951 (1970).

⁴C. C. Robinson and J. T. Fournier, *Chem. Phys. Lett.* **3**, 517 (1969); *J. Phys. Chem. Solids* **31**, 895 (1970).

⁵J. T. Fournier and R. H. Bartram, *J. Phys. Chem. Solids* **31**, 2615 (1970).

⁶C. C. Robinson, *J. Chem. Phys.* **54**, 3572 (1971).

⁷L. G. DeShazer, in *Optical Properties of Ions in Crystals*, edited by H. M. Crosswhite and H. W. Moos (Interscience, New York, 1967), p. 507.

⁸M. J. Weber, E. J. Sharp, and J. E. Miller, *J. Phys. Chem. Solids* **32**, 2275 (1971); M. J. Weber, *Phys. Rev. B* **4**, 2932 (1971).

⁹L. A. Riseberg and M. J. Weber, in *Progress in Optics*, edited by E. Wolf (North-Holland, Amsterdam, 1975), Vol. 14, and references cited therein.

¹⁰Yu. V. Denisov, I. V. Kovaleva, V. P. Kolobkov, and V. V. Rastoskuev, *Opt. Spectrosc.* **38**, 54 (1975).

¹¹A. Szabo, *Phys. Rev. Lett.* **25**, 924 (1970); **27**, 323 (1971).

¹²L. A. Riseberg, *Phys. Rev. Lett.* **28**, 789 (1972); *Solid State Commun.* **11**, 469 (1972); *Phys. Rev. A* **7**, 671 (1973).

¹³N. Motegi and S. Shionoya, *J. Lumin.* **8**, 1 (1973).

¹⁴W. M. Yen, S. S. Sussman, J. A. Paisner, and M. J. Weber, *Bull. Am. Phys. Soc.* **20**, 44 (1975).

¹⁵J. A. Paisner, S. S. Sussman, W. M. Yen, and M. J. Weber, *Bull. Am. Phys. Soc.* **20**, 447 (1975).

¹⁶T. Kushida and E. Takushi (unpublished).

¹⁷B. G. Wybourne, *Spectroscopic Properties of Rare Earths* (Interscience, New York, 1958), p. 708.

¹⁸M. T. Hutchings and D. K. Ray, *Proc. Phys. Soc. Lond.* **81**, 663 (1963).

¹⁹See, for example, C. Brecher, *J. Chem. Phys.* **61**, 2297 (1974).

²⁰H. Samelson, C. Brecher, and A. Lempicki, *J. Mol. Spectrosc.* **19**, 349 (1966).